Earth and Planetary Science Letters 540 (2020) 116261

Contents lists available at ScienceDirect

Earth and Planetary Science Letters

www.elsevier.com/locate/epsl

Deep slow-slip events promote seismicity in northeastern Japan megathrust

Mostafa Khoshmanesh [a,*], Manoochehr Shirzaei [b], Naoki Uchida [c]

[a] Department of Mechanical and Civil Engineering, California Institute of Technology, Pasadena, CA, USA
[b] School of Earth and Space Exploration, Arizona State University, Tempe, AZ, USA
[c] Graduate School of Science, Tohoku University, Sendai, Japan

ARTICLE INFO

Article history:
Received 13 July 2019
Received in revised form 24 March 2020
Accepted 2 April 2020
Available online xxxx
Editor: R. Bendick

Keywords:
slow-slip events
kinematic modeling
earthquake triggering
Japan subduction zone
repeating earthquakes
GPS

ABSTRACT

The sliding movement between oceanic and crustal plates in subduction zones is accommodated through both earthquakes and quasi-static or transient aseismic slip. On northeastern Japan megathrust, aseismic transients, known as slow-slip events, are suggested to precede and trigger major earthquakes in their immediate surroundings. However, the geodetic evidence for these episodic slow-slip events, as well as their link to the seismicity on neighboring locked segments of the megathrust, is missing. Here, we combine the on-shore geodetic data set with seismic observations during the interseismic period of 1996–2003 and demonstrate that episodic slow-slip events are prevalent across the down-dip portion (∼30–70 km depth) of the megathrust and the associated stress changes modulate the seismicity rate on the neighboring seismogenic zone. Consequently, small- to moderate-size earthquakes are periodically triggered, whose interaction through a domino effect might occasionally lead to major earthquakes. This observation has a profound impact on the estimation of seismic hazard in the region, introducing a new triggering mechanism that acts across the megathrust to the extent that has not been acknowledged before.

1. Introduction

At subduction zones, the general assumption is that seismic rupture and steady or transient aseismic slip, such as afterslip and slow-slip events (SSE), are distinct processes that occur on different areas of the fault zone (Avouac, 2015; Noda and Lapusta, 2013; Obara and Kato, 2016). Accordingly, subduction zone faults are conceived as several macrostructures, identified with distinct long-term behavior. These macrostructures are in turn characterized by different geometrical (Gao and Wang, 2014; Heuret et al., 2012; Tanioka et al., 1997) or frictional properties (e.g., Noda and Lapusta, 2013), being either velocity-strengthening (VS) or velocity-weakening (VW) in the framework of the rate-and-state friction law (Dieterich, 1979; Ruina, 1983). In this perspective, the VS aseismic (i.e., creeping) segments are considered to act as barriers, inhibiting earthquake rupture that commonly initiates on the VW seismic sections from further propagation. However, depending on their size, the frictional properties, and the average interseismic coupling, seismic ruptures may break into these rupture-impeding segments (Kaneko et al., 2010). Moreover, temporary acceleration of creep rate in the form of SSEs has been shown to occur on the creeping segments and modulate the timing of earthquakes on nearby locked zones (Khoshmanesh and Shirzaei, 2018a; Schurr et al., 2014; Socquet et al., 2017). Therefore, a successful effort to predict the extent and timing of seismic rupture requires identification and detailed understanding of the interaction between adjacent macrostructures.

On the northeast Japan subduction zone (NJSZ), the spatial distribution of long-term coupling, constrained by either geodetic (e.g., on-shore Global Positioning System (GPS)) or seismic (e.g., repeating earthquakes) data sets suggest that, consistent with the general assumption, the subducting fault partitions into several major creeping and locked macrostructures (Hashimoto et al., 2009; Igarashi, 2003; Loveless and Meade, 2010; Suwa et al., 2006). According to these coupling models, there are two persistent creeping sections in the deep (> ∼30 km) segments of NJSZ: to the north, near the shore of Iwate prefecture in northern Honshu, and to the south, off the shore of Ibaraki prefecture. The deep zone in the central section of the fault, near the shore of Miyagi and Fukushima prefectures, however, is characterized by high coupling during the interseismic period and is suggested to host several locked asperities that have generated large (M7+) historic earthquakes (Shibazaki et al., 2011; Yamanaka and Kikuchi, 2004)

* Corresponding author.
E-mail address: mkh@caltech.edu (M. Khoshmanesh).

https://doi.org/10.1016/j.epsl.2020.116261

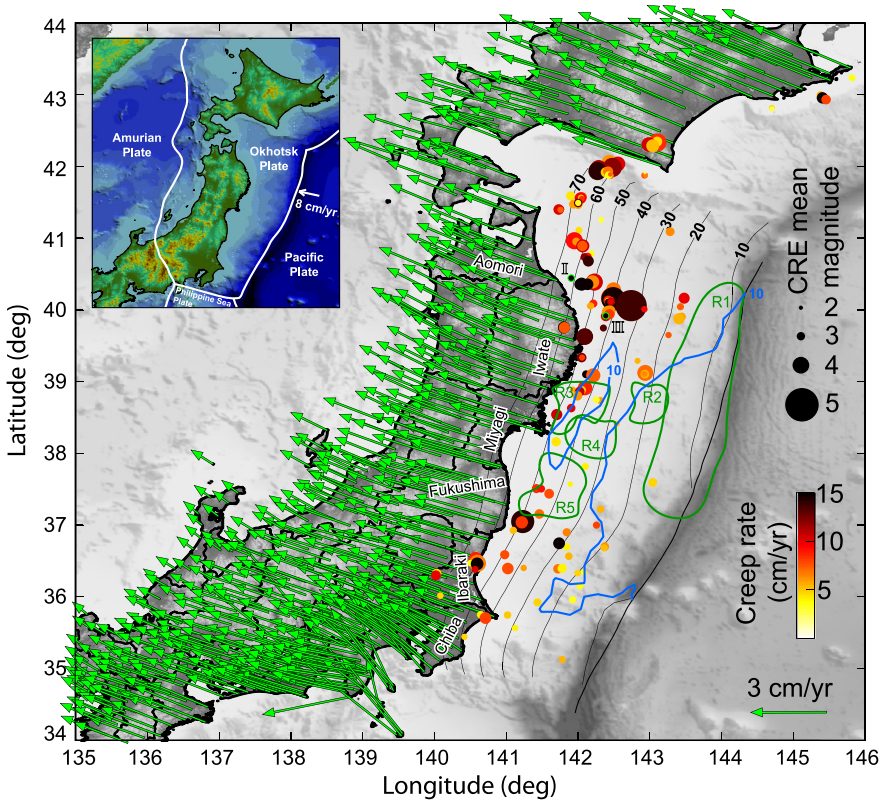

Fig. 1. Study Area and observations. The long-term rate of GPS displacements during 1996–2003, corrected for the common-mode and seasonal errors, is shown using the green arrows. The solid circles show the location of CRE sequences detected during 1996–2003 (Uchida and Matsuzawa, 2013). Size and color of each circle represent the mean moment magnitude and the long-term creep rate of each CRE sequence, respectively. The time series and estimated long-term rate of the two CRE sequences identified with I and II is shown in Fig. S2. The blue contour shows the area of 10-m-coseismic-slip of the Tohoku earthquakes based on the model from Shirzaei et al. (2014). The thin black lines show the depth contour lines on the subducting slab and the outlines of historical earthquake rupture areas is plotted in green (Shibazaki et al., 2011). R1: 1611 M_w8.1; R2: 18 January 1981 M_w7.1; R3: 12 June 1978 M_w7.8; R4: 1936 M_w7.4; R5: 1938 M_w7.3. Inset: the location and tectonic setting of Japan, lying at the intersection of Pacific, Okhotsk, Philippine Sea, and Amurian plates. (For interpretation of the colors in the figure(s), the reader is referred to the web version of this article.)

(Fig. 1). The shallow portion of the NJSZ, except for a small zone off the shore of Iwate prefecture that might be slightly creeping (Uchida et al., 2016), is suggested to be highly coupled during the interseismic period. Significant tsunamigenic events have ruptured the shallow segment in the past, particularly in the central part (Shibazaki et al., 2011; Yamanaka and Kikuchi, 2004), including the 2011 M_w9.0 Tohoku earthquake (Shirzaei et al., 2014; Simons et al., 2011).

As the primary goal of this study, here we use a combination of repeating earthquake data set alongside on-shore GPS daily observations to investigate the time evolution of interseismic fault creep during 1996–2003 and constrain the location of long-term creeping and locked macrostructures on the NJSZ. Enabled by the daily kinematic model of creep on the fault, we then provide evidence for periodic SSEs on the down-dip creeping section of the NJSZ and investigate their link to the seismicity on neighboring locked macrostructures. Finally, motivated by our results and the previous observations of distinct faulting processes that coexist on the same portion of the NJSZ, we propose a conceptual model for NJSZ in the context of rate and state friction law, which might unify the macrostructural perspective of the subducting fault with the intricate microstructural pattern, suggested by these observations.

2. Data and methods

The Japan subduction zone is an extremely well-instrumented plate boundary, being monitored by the Japan Meteorological Agency (JMA) seismic network as well as the GPS Earth Observation Network (GEONET), which comprises over 1200 stations (Sagiya, 2004; Sagiya et al., 2000). This monitoring effort is motivated by the fact that Japan is a seismically active region, lying on the intersection of four tectonic plates: Pacific, Okhotsk, Amurian, and Philippine Sea (Fig. 1 inset). Subduction of the Pacific plate beneath the Amurian microplate with a rate of 8 cm/year has been the source of major tsunamigenic seismic events on the NJSZ, such as the 2011 M_w9.0 Tohoku earthquake (Fig. 1). Here, we use the GPS daily solutions for GEONET stations, provided by Ozawa et al. (2012), and the Characteristically Repeating Earthquake (CRE) dataset from the study by Uchida and Matsuzawa (2013) to constrain the spatiotemporal distribution of creep on the NJSZ. We focused our analysis on the interseismic period of 1996–2003 when there were no earthquakes larger than M6.5 on the NJSZ. The termination of this interseismic period is marked by the M_w8.3 Tokachi-Oki earthquake that occurred on 25 September 2003 near the northern boundary of our study area (Miyazaki and Larson, 2008). Therefore, observations between 21 March 1996, which is the earliest measurement in the GPS dataset, and 24 September 2003 are considered. Observations from 197 CRE sequences and daily horizontal displacement time series recorded by 961 GPS stations, with at least one year of observation and less than 0.2 years data gap, are used in a time-dependent inversion scheme to determine the daily distribution of creep (Fig. 1). A triangular mesh (Fig. S1), based on the fault geometry from Slab1.0 (Hayes et al., 2012), is used to represent the subducting plate in the inversion, as well as for the refinement of both datasets. Moreover, we also quantified the times series of seismic activity using the JMA seismic catalog in order to investigate the role of interseismic creep and its transient variations in triggering earthquakes on NJSZ. In particular, the seismic moment release, earthquake count,

and Gutenberg-Richter b-value is estimated and compared to the Coulomb stress variations resulting from creep rate changes.

2.1. Characteristically repeating earthquakes

Characteristically Repeating Earthquakes (CREs) are thought to be associated with the repeated failure of relatively small asperities, occupying less than 1% of the active fault surface, loaded by the surrounding aseismic slip (Nadeau et al., 1994; Nadeau and Johnson, 1998). The seismic moment release provides quantitative information about the amount of aseismic slip involved in these seismic events. Using cross-spectral analysis, Uchida and Matsuzawa (2013) identified CREs on the northeast Japan subduction zone, beginning in 1984, and grouped them into CRE sequences occurring at discrete locations on the subducting plate interface. The down-dip extent of the CREs limits to ~65 km depth. The location and long-term creep rate inferred from CREs for the interseismic period of 1996–2003 are shown using solid circles in Fig. 1. The unusually high creep rate estimated from CREs at some locations might be due to the localized stress perturbations resulting from nearby repeating events and larger earthquakes. Moreover, failure in distinguishing the nearby repeating events from truly overlapping events might lead to the overestimation of associated creep rates in those locations (Uchida and Bürgmann, 2019). These uncertainties might lead to disagreement between creep estimated from CREs and that obtained from geodetic observations, which have been pointed out in previous studies (e.g., Khoshmanesh et al., 2015; Shakibay Senobari and Funning, 2019).

In order to use the CRE observations to invert for a daily creep distribution on the fault mesh through time-dependent inversion, we interpolated the dataset over time. To this end, first, the long-term creep rate per CRE sequence is estimated through linear regression (Fig. S2), considering sequences with more than three events (Fig. 1). The estimated long-term rate is then used to obtain a time series of daily creep at the location of each CRE sequence. Therefore, no temporal variation is present in the interpolated time series of CRE-creep for each sequence. Next, we spatially oversample the obtained sparse time series to assign a daily CRE-creep to the triangular patches that have at least one CRE sequence within their 50 km radius (Supplementary Text S1 and Figs. S3-S4).

2.2. Global positioning system

Here we use the GPS daily times series of GEONET stations from Ozawa et al. (2012), provided in the stable Eurasian reference frame after Apel et al. (2006). Only the horizontal components are considered in this study, due to the low signal to noise ratio of the vertical component and the contribution from subduction erosion that adds additional complexity to the vertical deformation data (Heki, 2004). To isolate the signal due to creep, we implement a refinement procedure, through which we remove the effect of the common-mode error and seasonal variations. The common-mode error is a noise in the GPS time series, which is not related to the tectonic movements and is common to all the stations within the network (Wdowinski et al., 1997). A spatial filtering technique based on a Helmert transformation (Mavrommatis et al., 2014) is used to remove this error from the GPS time series (Supplementary Text S2 and Figs. S5-S7). Next, the seasonal signal in the GPS time series is removed using a stochastic method based on Kalman Filtering (Davis et al., 2012), which estimates the time-varying linear trend and harmonic coefficients for each station (Supplementary Texts S3-S4 and Figs. S8-S9). The green arrows in Fig. 1 and Fig. S10 show the long-term rate of GPS stations relative to the Amurian plate (Fukue station), estimated through linear regression of the corrected time series.

The spatial gradients of corrected GPS observations are estimated to obtain a first-order approximation of the spatiotemporal variability of the fault coupling along the NJSZ, following the work by Uchida et al. (2016) (Supplementary Text S5). This approach provides some insight into the fault coupling at the deeper portion of NJSZ, in areas that are closer to the on-shore GPS stations. A stronger fault locking at the deep seismogenic segment causes a larger westward displacement, especially at the location of GPS stations closer to the trench. However, the GPS stations on the western part of the Honshu, located above the deep ductile creeping portion of the subducting slab, are less sensitive to the coupling of the seismogenic section. Therefore, the spatial gradients of long-term and short-term GPS velocities can be used as a proxy for the location of locked and creeping segments of subducting fault and creep rate variations, respectively.

2.3. Time-dependent slip inversion

To assess the model of interseismic creep on the NJSZ we used the concept of backslip inversion (Savage, 1983). In this approach, the entire subduction zone up to a depth of ~700 km, represented by the Slab1.0 model (Hayes et al., 2012), is allowed to slip at its long-term rate of 8 cm/year and the deformation time series at the location of GPS stations are estimated using a forward modeling (Fig. S11). By subtracting the modeled values from the actual displacements (Fig. S12), observed by the GPS stations and corrected for the common-mode and seasonal error, we then solve for the daily time series of creep on the shallow ($< \sim 80$ km) segment with opposite sign, as if the subduction zone undergoes a hypothetical slip with normal sense. To associate the observations, comprised of backslip GPS displacements (Fig. S12) and CRE-creep with this shallow creep, we use a time-dependent inverse modeling scheme (Khoshmanesh et al., 2015; Shirzaei and Bürgmann, 2013; Shirzaei et al., 2014) that solve for a static creep distribution for each time step (i.e. every day). The creep (C_t) on each patch at each time step ($t = 1, \ldots, n$) is related to the observations, $L_t = [L_x, L_y, L_c]^{\mathrm{T}}$ as follows:

$$\begin{bmatrix} L_x \\ L_y \\ L_c \end{bmatrix}_t + \begin{bmatrix} v_x \\ v_y \\ v_c \end{bmatrix}_t = BC_t,\ P_t = \begin{bmatrix} \sigma_{0_x}^2 I & 0 & 0 \\ 0 & \sigma_{0_y}^2 I & 0 \\ 0 & 0 & \sigma_{0_c}^2 P_c \end{bmatrix} \tag{1}$$

where, x, y, and c indices refer to the easting and northing components of GPS displacement and CRE-creep observations, respectively, $v_t = [v_x, v_y, v_c]^{\mathrm{T}}$ is the vector of observation residuals, and B is the Green's functions matrix. The Green's function used for both inversion and forward modeling of horizontal GPS observations, mentioned above, is estimated assuming dip-slip motion on triangular patches buried in an elastic, homogeneous half-space medium (Meade, 2007) with a Poisson ratio of 0.25. The matrix B also includes the Green's function for CRE-creep observation, which is a matrix of size $n_r \times n_c$, where n_r is the number of patches with a CRE-creep assigned to them out of total n_c patches making up the fault (Fig. S4A). For each row of the matrix, the column corresponding to the same patch in the vector of unknowns is one and zero elsewhere. The weight matrix (P_t) is scaled with a separate primary variance factor (σ_0^2) for each set of observations to determine the relative weight between them. Here we considered $\sigma_{0_x}^2 = 4$, $\sigma_{0_y}^2 = 2$, and $\sigma_{0_c}^2 = 1$. It should be noted that the east components of the GPS data are given more weight relative to the north components, as the convergence rate is predominantly east-west, and thus the signal to noise ratio for the north component is smaller than that for the east component. Moreover, the CRE-creep observation has the least weight among observation, due to lack of temporal variability in the interpolated CRE observation and higher

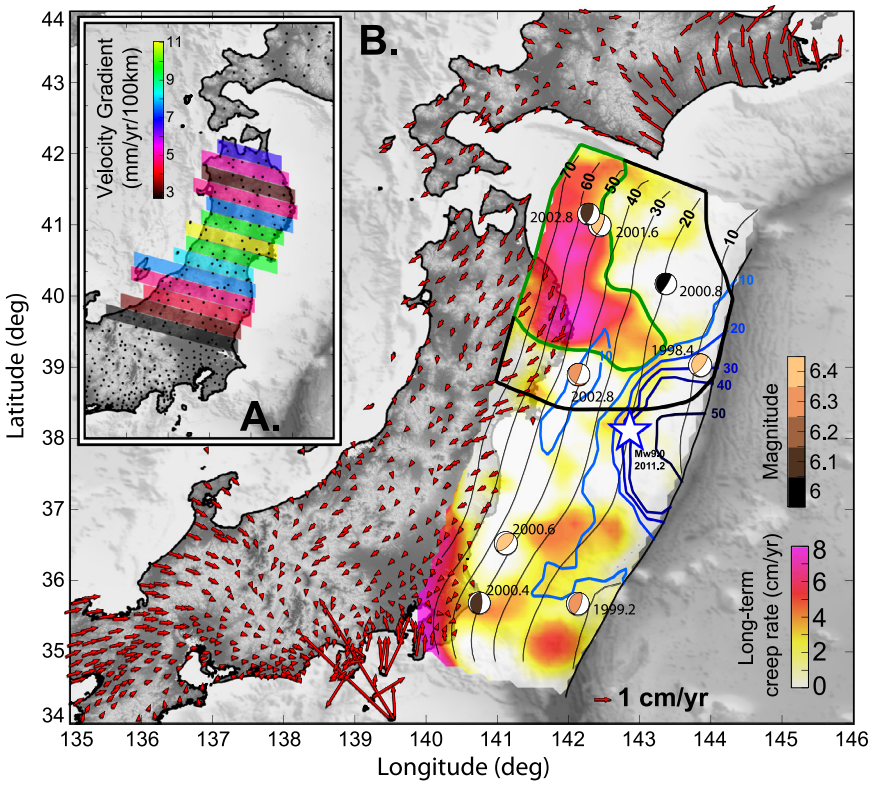

Fig. 2. Interseismic creep distribution. (**A**) Spatial gradient of GPS long-term velocities along 40-km-wide profiles on central and northern Honshu. (**B**) The spatial distribution of long-term creep rate during 1996–2003 on the NJSZ, constrained using both GPS and CRE observations. The beach balls show the location and focal mechanism of M6 earthquakes that occurred during 1996–2003, color coded according to their moment magnitude. Blue contour line represents the coseismic rupture area of the Tohoku earthquake based on the model from Shirzaei et al. (2014). The white star shows the hypocenter of this earthquake. The creeping segment, comprised of the patches with long-term rates higher than 3 cm/year, and surrounding locked area, with annual Coulomb stressing rate of 0.5 KPa/year or higher, are enclosed by the green and black curves, respectively. The red arrows represent the model residual, obtained as the difference between original (Fig. S12) and modeled backslip long-term GPS observations.

uncertainty inherent in these observations. Nonetheless, we also tested equal weight between east and north component ($\sigma_{0_x}^2 = 2$, $\sigma_{0_y}^2 = 2$, and $\sigma_{0_c}^2 = 1$), as well as between east component and CRE observation ($\sigma_{0_x}^2 = 2$, $\sigma_{0_y}^2 = 1$, and $\sigma_{0_c}^2 = 2$). The relative weight of CRE-creep between different patches (P_c) is assigned using the estimated standard deviation (Fig. S4B). For the GPS time series (both X and Y components), however, a uniform weight is assumed for all the GEONET stations, determined by the identity matrix (I) in the associated components of the weight matrix. To remove the possible outliers, a spatial median filter (Hammond et al., 2016) is applied to the GPS data set, which replaces the daily X and Y displacements of each GPS station with the median value of nearby stations found using Delaunay triangulation.

Equation (1) is solved subject to a reweighted L2-norm minimization of the observation residuals, whereby following each iteration, the observations are reweighted based on the residuals from the previous iteration (Shirzaei and Bürgmann, 2013). This approach allows the minimization of the effect of outliers and other observation artefacts (O'leary, 1990). The unknowns (C_t), consisting of the daily backslip creep, are also bounded during inversion to be within -10 and 10 times that associated with the long-term convergence rate (8 cm/year) for one day. This choice of bounds enables us to detect short-term creep rate variation, with rates up to 10 times that of tectonic rate. In the inversion step, we also minimize the second-order derivative of the creep distribution in each time step to reduce the roughness of the slip (Harris and Segall, 1987) using equation $\gamma DC_t = 0$, where D is the Laplacian operator, and γ is the smoothing factor, which determines the roughness of the optimum creep model. The optimum γ, estimated as the point of maximum curvature of the trade-off curve between model roughness and norm of residuals (Shirzaei and Bürgmann, 2013), is determined to be 50 (Fig. S13).

3. Results

3.1. Fault coupling along NJSZ

The estimated spatial gradient of long-term GPS velocities in northern and central Honshu (Fig. 2A) suggests that, in agreement with the previously published coupling maps of NJSZ (Hashimoto et al., 2009; Igarashi, 2003; Loveless and Meade, 2010; Suwa et al., 2006), the coupling in northern and southern parts of the fault is lower relative to the central portion. To further investigate the interseismic fault coupling, we invert the long-term horizontal displacement rate of GEONET stations (by setting $\sigma_{0_c}^2 = 0$ in Eq. (1)) for the average interseismic creep rate on the fault. The obtained result (Fig. S14) reveals a locked section in the central part and two creeping segments to the north and south, confirming the expected fault coupling pattern inferred from the long-term velocity gradients of on-land GPS stations (Fig. 2A). Adding the CRE observations does not change the location of the locked and creeping sections but adds to their size and the spatial complexity of the model (Fig. 2B). Moreover, the overall pattern of coupling seems to be independent of the relative weight between different observations (Fig. S15). Nonetheless, increasing the weight of CRE observations results in an overall decrease in the degree of coupling along the fault (Figs. S15), because some estimates of creep rate obtained from raw CREs are unusually high and up to 15 cm/year (Fig. 1 and S4).

We find that the area that accommodated the coseismic slip (>10 m) of the 2011 Tohoku earthquake is characterized by near-

zero creep predicted by our model, marking a locked fault segment within 36° to 39° latitude and depths shallower than ~30 km (Fig. 2B). This locked segment is adjacent to a deep fast creeping portion to the north (enclosed by the green curve in Fig. 2B), near the shore of Aomori and Iwate prefectures that aseismically slips by an average rate up to 8 cm/year throughout the interseismic period. The up-dip area of this creeping segment shows almost no creep during the interseismic period but later hosted postseismic slip due to the 2003 M_w8.3 earthquake (Miyazaki and Larson, 2008). Another creeping segment is located in the southern part of our study area, near the shore of Ibaraki and Chiba Prefectures. The shallow portion of this southern segment also contains three smaller creeping zones. However, since the GPS displacement observations in this area are also affected by the movement between the Philippine Sea and Okhotsk Plates, which adds to its complexity, we do not include this segment in our further analysis.

It is noteworthy that the resolved high coupling in the shallow portions of the megathrust, near the trench, might also be related to the lower sensitivity of the on-shore geodetic observation to slip on this area (Loveless and Meade, 2010). Adding CRE observations can reduce the uncertainty, albeit in the deeper portion, where most of the observed CRE sequences are located (Fig. 1 and S4). Nonetheless, lack of the repeater activity on the shallow megathrust can be indicative of the high degree of coupling during the interseismic period (Uchida and Bürgmann, 2019).

3.2. Temporal variations of creep rate

The temporal variations of creep rate on the NJSZ, in particular, within the northern creeping segment, is evident in the time series of the spatial gradient of short-term velocity for on-shore GPS stations that locate inside the four northern profiles (Fig. S16). These profiles are chosen due to their proximity to the northern creeping segment, which is also evident in their relatively lower long-term velocity gradient (Fig. 2A). To further investigate the temporal variation of interseismic creep on the subducting slab, we invert for the daily slip time series for the period 21 March 1996 to 24 September 2003. We use a combination of the daily solutions of GPS horizontal components, corrected for the common-mode error and seasonal signals (Section 2.2), and the CRE dataset, oversampled on the triangular fault patches (Section 2.1 and Fig. S4). Provided the optimum creep model, the synthetic displacement time series agrees well with that of GPS observations (Figs. S17-S18), with an average standard deviation of 1 mm for both X and Y components (Figs. S19-S20). Note that the disagreement between modeled and original observation in some days (Figs. S19-S20) results in locally large misfits, which are propagated forward and cause a slight discrepancy in the cumulative displacements of some stations (Figs. S17-S18). The possible causes of the localized large misfits include the choice of bounds for the daily creep, noise of the GPS observations, and also the unmodeled creep on the other fault segment that has not been considered in this study.

To investigate the short-term creep rate variation, focusing on the northern creeping segment (inside green curve in Fig. 2B), we spatially average the cumulative creep, which improves the signal to noise ratio (Fig. S21). The time series of short-term creep rate (Fig. 3A), estimated using this average cumulative creep, shows variations with an almost semi-annual cycle. This creep rate variation is also evident in the spatial distribution of cumulative creep in three-months moving windows during 1996.25–2003.75 (Fig. S22). Since the GPS displacement time series are corrected for any annual and semi-annual artefacts as well as common-mode error, the observed cyclic creep rate variations are not likely due to these errors in the GPS measurements. Therefore, we suggest that these

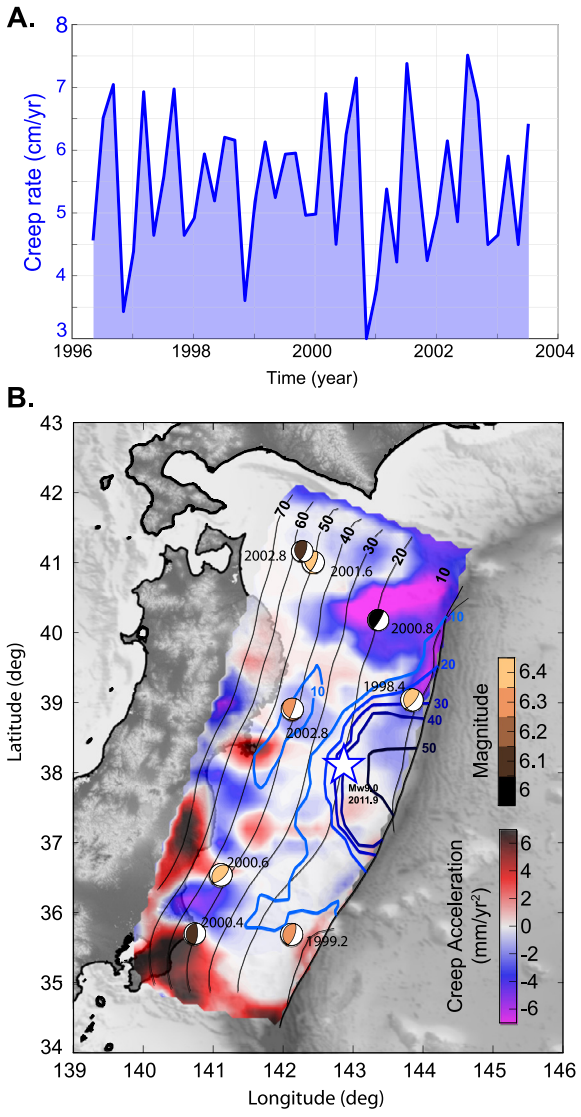

Fig. 3. Creep rate variations. (**A**) Temporal evolution of average creep rate within the northern creeping segment estimated using a three-month moving window with a step size of two. (**B**) The spatial distribution of estimated constant acceleration along NJSZ. The blue contour line and beach balls are the same as in Fig. 2B.

creep rate changes are indicators for periodic SSEs that occur on the creeping segment. Also, comparing the creep rate evolution, with that obtained in Uchida et al. (2016), using the CRE observations for a smaller area near-shore of Iwate Prefecture shows an overall good agreement between the two (Fig. S23). To explain the minor discrepancy, especially between 2001 and 2002, we note that the creep rate time series in the present study are averaged over a larger area compared to that of Uchida et al. (2016). Moreover, the temporal resolution of each CRE sequence in Uchida et al. (2016) is in the order of several months or years (Fig. S2), whereas the GPS observations, used to constrain the creep rate changes in the present study, have a daily temporal resolution. Therefore, using GPS, we were able to detect short-term creep rate variation, which might be hard to achieve using the CRE observations alone.

Earlier studies on the interseismic creep in NJSZ (Mavrommatis et al., 2014; Yokota and Koketsu, 2015) and San Andreas Fault (Khoshmanesh and Shirzaei, 2018b) provided evidence for a decadal-scale acceleration before large earthquakes. To estimate such long-term transients from the optimum creep model, we fit

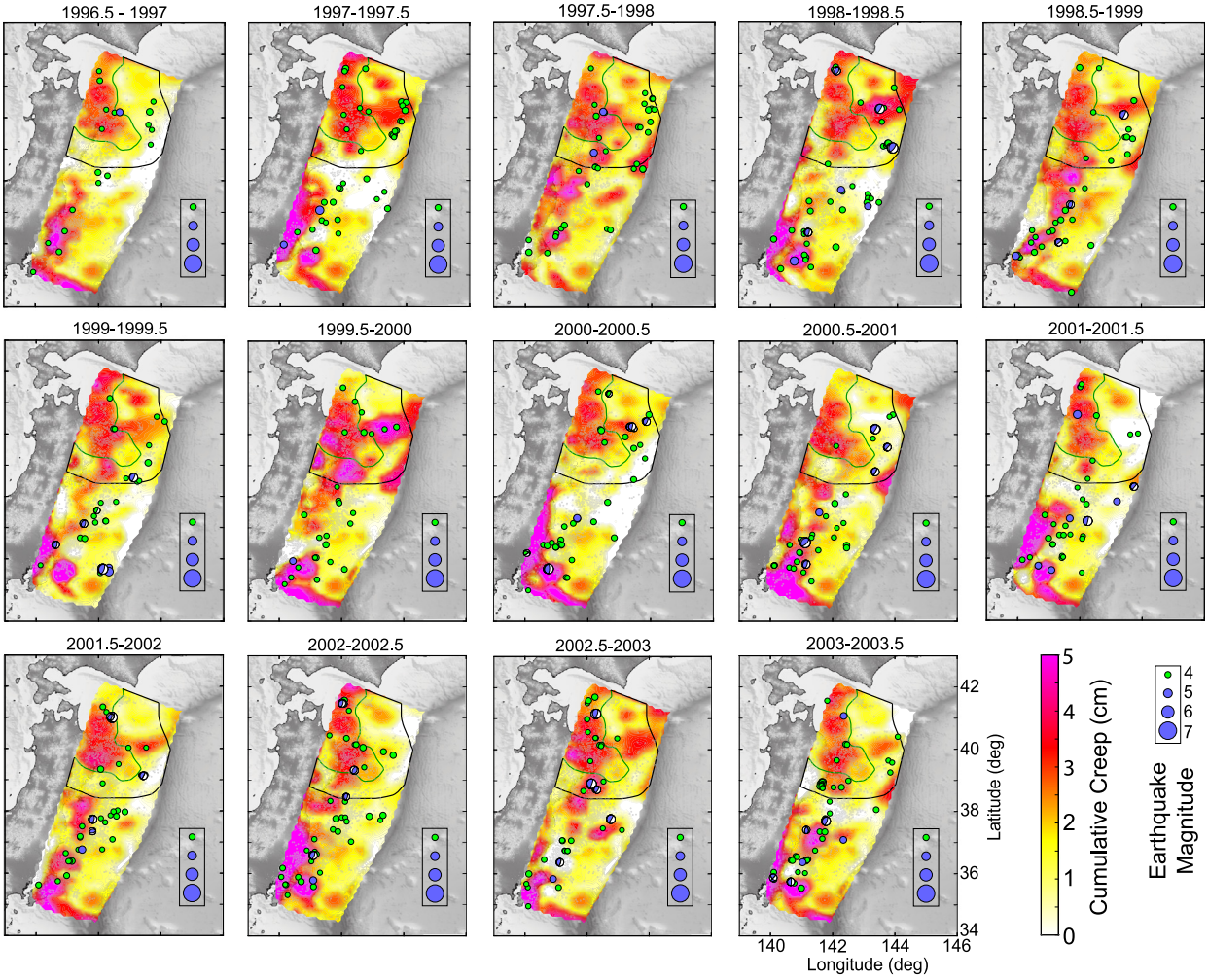

Fig. 4. Spatiotemporal evolution of creep on NJSZ. Cumulative creep and seismicity within six-months moving windows. The M4 and M5+ earthquakes are shown using solid green and blue circles, respectively. Wherever available, the focal mechanism of earthquakes is shown using the beach balls. The limits of the northern creeping segment and surrounding locked zone, as shown in Fig. 2B is also shown for each panel to enable a visual comparison between the short-term and long-term results.

the equation $d(t) = v_0(t - t_0) + \frac{1}{2}a(t - t_0)^2$ to the obtained time series of creep. In this equation, $d(t)$ is the cumulative creep at time t relative to reference time t_0, and unknowns are the initial velocity (v_0) and constant acceleration (a). The results (Fig. 3B) show an intricate distribution of decadal acceleration (a) along the NJSZ, with an overall change in the sign of acceleration moving from north to south. In particular, there is a fast deceleration zone, extending from the trench to depth of ~40 km at 39°–41° latitude, which might be associated with the decaying postseismic deformation of 1994 M_w7.7 Sanriku earthquake. The interseismic creep in the northern creeping segment, however, seems to be lacking a long-term transient signal. Moreover, the maximum acceleration occurs in the deep portion (>60 km) of southern parts of the NJSZ at 35°–37° latitude, and on the very southern portion of the fault. However, as mentioned earlier, the creep time series obtained for this part of the fault is less reliable due to the scarcity of CRE observations (Fig. 1 and S4) and the movement between the Philippine Sea and Okhotsk Plates affecting the on-shore GPS observations. Note that the large-scale creep transient prior to the 2011 M_w9.0 Tohoku earthquake, discussed in previous studies (Mavrommatis et al., 2014; Yokota and Koketsu, 2015) most possibly started in ~2002 (Yokota and Koketsu, 2015) and is absent in our creep acceleration map, which corresponds to the time interval 1996–2003.

4. Discussion

4.1. Interaction between SSEs and seismicity

Visual inspection of the location of M6 earthquakes within the interseismic period on the NJSZ shows that they occur within the periphery of, or outside, the long-term creeping zones (Fig. 2B). Moreover, the temporal evolution of interseismic creep and seismicity in six-months moving widows reveals that although the creep distribution is not always confined to the long-term creeping segment, the majority of M5+ earthquakes occur in the locked area adjacent to the transient creep (Fig. 4). This observation suggests that the shear stress change due to creep and SSEs possibly loads the adjacent locked asperities (Hirose et al., 2010). Furthermore, the distribution of M6 earthquakes during 1996–2003 compared with the map of long-term acceleration (Fig. 3B) indicates that all these events occurred either on the decelerating parts or the transition between accelerating and decelerating zones. This observation may further support the idea that the imparted stress due to long-term creep acceleration possibly enhances the earthquake rupture on a decelerating segment, which has been accumulating strain over the years (Khoshmanesh and Shirzaei, 2018b; Mavrommatis et al., 2014).

To investigate the impact of SSEs that occur inside the northern creeping segment on the seismic activity of the neighboring

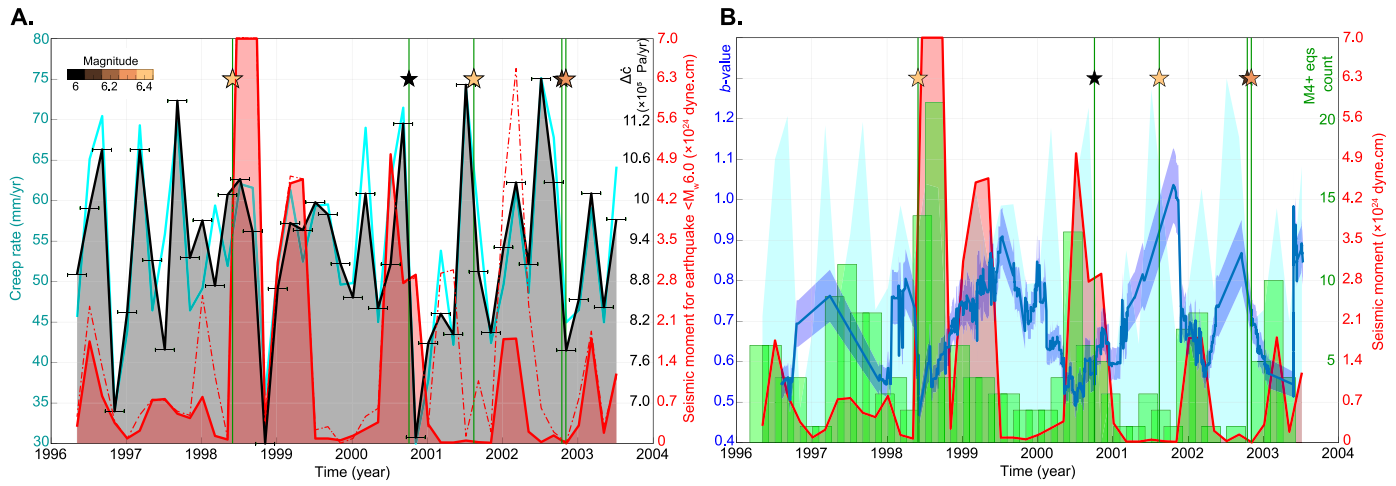

Fig. 5. Interaction of SSEs and seismicity. (**A**) Temporal evolution of average creep rate within the northern creeping segment (cyan), as well as Coulomb stressing rate (black) and total seismic moment (red) in the neighboring locked segment. The red dashed line shows the time series of total seismic moment when the seismicity inside the creeping segment is added to that of neighboring locked segment. A temporal moving window of three months width (horizontal black error bar on Coulomb stressing rate curve) and step size of two months is used. The value associated with each moving window is displayed in its middle point. Green vertical lines indicate the timing of M6 earthquakes, shown using the stars and color-coded by their moment magnitude. (**B**) Temporal evolution of M4+ earthquakes count and the Gutenberg-Richter *b*-value in the neighboring locked segment, compared with time series of seismic moment release. The time series of creep rate is also shown in the background using cyan shaded area.

long-term high-coupling parts of the NJSZ, we estimate the time series of Coulomb failure stress change (ΔC) at the center of fault patches located outside this creeping zone (Supplementary text S7 and Fig. S24). Focusing on the fault patches surrounding the northern creeping segment, with annual Coulomb stressing rate of 0.5 KPa/year or higher (black curve in Fig. 2B), the time series of total $\Delta\dot{C}$ increases intermittently (Fig. 5A), consistent with that of SSEs (Fig. 3A). We further investigated the correspondence between the time series of the total seismic moment of earthquakes smaller than M6 within 15-km-distance of the adjacent locked segment and the associated Coulomb stressing rate change (Fig. 5A). The comparison suggests that all the spikes in the seismic moment release correspond to the temporary increase of the Coulomb stressing rate due to SSEs on the creeping segment. Adding the seismic moment associated with the earthquakes within the creeping segment (Fig. S25) to that of adjacent locked segment results in an even better agreement between the timing of SSEs and earthquake activity (Fig. 5A and S26). Moreover, most of the M6 earthquakes occur within the time window of increased Coulomb stressing rate. This observation may suggest a causal relationship between SSEs on the northern creeping segment and seismicity, especially on the nearby locked portion of the NJSZ.

We further evaluate the time series of Gutenberg-Richter *b*-value (Gutenberg and Richter, 1944) using the seismic records within 15-km-distance of the adjacent locked segment (Supplementary Text S6). The *b*-value time series shows the temporal evolution of the ratio of smaller to larger earthquakes, which is inversely proportional to the effective normal stress on the fault (Khoshmanesh and Shirzaei, 2018a; Schorlemmer et al., 2005; Tormann et al., 2013). The temporal pattern of estimated *b*-value time series is negatively correlated with the total seismic moment as well as the number of M4+ earthquakes (Fig. 5B). Considering the correspondence between Coulomb stress (creep rate) and seismic moment (Fig. 5A), this observation suggests that the SSEs on the down-dip creeping segment often cause a proportional increase in the number of large earthquakes within the neighboring locked region, decreasing the *b*-value. The time variation of *b*-value is also suggested to be caused by the temporary change in the mechanism type of earthquakes from thrust to normal after large earthquakes, such as the 2011 M_w9.0 Tohoku earthquake (Bürgmann et al., 2016). This, however, is less likely to be a major factor in the *b*-value changes observed here, due to the absence of particularly large earthquakes in our study period.

4.2. Microstructures on megathrust

Here it has been shown that the acceleration of creep in the form of SSEs on the northern creeping segment might periodically modulate the seismic activity in the adjacent locked area of the NJSZ. However, focusing on the long-term creeping and locked macrostructures, the interaction between SSEs in the former and seismicity in the latter is not entirely straightforward, as suggested by the lack of seismicity elevation during some of the SSEs and occurrence of two M6 events during non-peak Coulomb stress periods (Fig. 5). One of these two M6 events is happening inside and close to the edges of, and the other one outside, the creeping segment, both adjacent to a zone of localized accelerated creep (see panel 2002.75–2003 of Fig. S22). Therefore, the transient creep is not strictly limited to the northern creeping section; it might sometimes happen in part of the creeping segment and also in the surrounding long-term high-coupling area and trigger earthquakes in their vicinity, as is evident in the spatiotemporal distribution of creep (Fig. 4 and Fig. S22). Some authors have previously provided evidence for several episodes of SSE in the locked segment of NJSZ that ruptured during the 2011 Tohoku earthquake (Ito et al., 2013; Kato et al., 2012; Uchida et al., 2016) and accommodated several historic M7+ seismic events (Shibazaki et al., 2011; Yamanaka and Kikuchi, 2004) (Fig. 1). One such SSE that initiated ~20 days before the event, likely triggered the 2011 M_w9.0 earthquake (Kato et al., 2012). This locked zone also hosted other types of aseismic transients, such as the postseismic slip of the 2003 M_w8.3 (Miyazaki and Larson, 2008) and 2011 M_w9.0 earthquakes (Fukuda et al., 2013; Shirzaei et al., 2014).

Moreover, the northern long-term creeping segment is not entirely devoid of seismic asperities, and as evident from the distribution of seismicity (Figs. 2, 4, S22), several M5+ earthquakes have occurred in this area. It is also in agreement with Uchida et al. (2016), which suggested that part of the northern creeping segment, near the shore of Iwate, includes some seismic asperities, capable of M5+ earthquakes that are triggered by SSEs in this zone. This evidence of distinct modes of slip coexisting on the same fault segment and their complex interaction can challenge

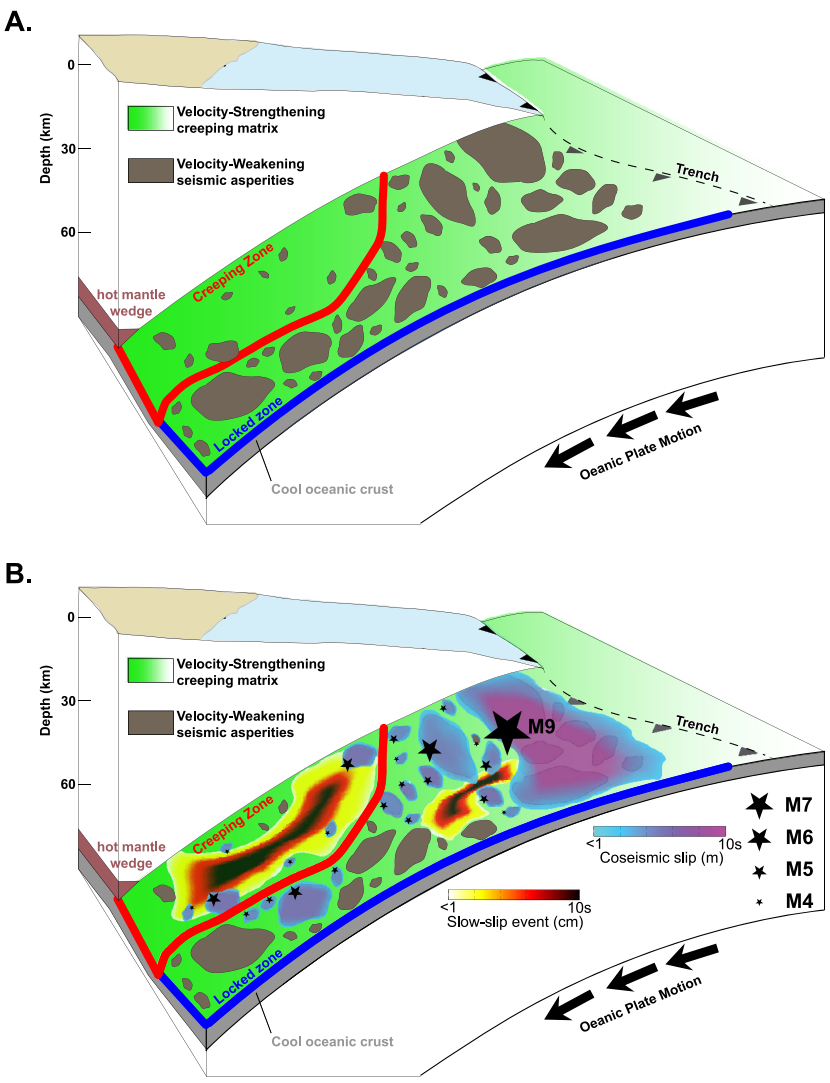

Fig. 6. Conceptual model of northeast Japan megathrust based on rate-and-state law. (**A**) The general setting, showing distribution of velocity-weakening asperities of different size (dark brown patches) embedded in the velocity-strengthening creeping matrix, shown in green. The deep creeping zone, hosting the periodic slow-slip events, and the neighboring locked segment, which is the rupture zone of major earthquakes, are indicated with red and blue lines, respectively. (**B**) Slow-slip event in the creeping zone triggers isolated failure of asperities, generating small- to moderate-size earthquakes on the neighboring locked segment. Efficient interaction between smaller earthquakes might generate enough stress perturbation through a domino-effect and leads to rupturing of bigger asperities, causing major earthquakes. Though these two scenarios are not necessarily happening at the same time but are shown in the same panel. Smaller SSEs can also occur in the creeping matrix, outside the main creeping segment and trigger earthquake in their immediate surroundings.

the macrostructural perspective that grossly divides the fault zone into major seismogenic and aseismic segments (e.g., Noda and Lapusta, 2013).

As an alternative hypothesis, we suggest that the megathrust might be paved with individual asperities, namely localized high frictional strength (competent) contact areas of different size that are capable of seismic rupture, embedded in the low strength (incompetent) creeping area, which act as seismic barriers (Lay et al., 1982) (Fig. 6A). This hypothesis is supported by the field observations of exhumed subduction zones, which suggest that isolated clusters of competent material of different scales are embedded within incompetent gouge matrix, forming a mélange of variable frictional strength (Bebout and Barton, 2002; Fagereng, 2011; Fagereng and Sibson, 2010; Meneghini et al., 2010). The high-frequency seismic waves recorded during the 2011 Tohoku earthquake also point to the intricate rheology of fault material (Meng et al., 2011).

The suggested intricate microstructure of the megathrust can be further elaborated according to the rate-and-state friction law, in particular, the $a-b$ parameter, which determines the change of friction coefficient in response to variations of loading rate in the steady-state condition (Dieterich, 1979; Ruina, 1983). A negative $a-b$, known as VW properties, is required for the frictionally unstable regime, corresponding to the seismogenic asperities (Chen and Lapusta, 2009; Dublanchet et al., 2013; Noda and Lapusta, 2013). Whereas, the creeping matrix of the fault is characterized by VS or weak VW properties, indicated by positive or small negative $a-b$, respectively (Scholz, 1998) (Fig. 6A). In case of VS, the matrix is stably creeping in the absence of external stress perturbation, and is also capable of hosting aseismic transient slip through either SSEs or afterslip, if subject to stress perturbation caused by, e.g., nearby earthquakes or transient pore fluid pressure elevation (Khoshmanesh and Shirzaei, 2018a; Perfettini and Ampuero, 2008). A small negative $a-b$, in combination with elevated fluid pressure, has also been suggested to be a favorable condition for SSE (Leeman et al., 2016; Liu and Rice, 2007). The condition required for aseismic transients is also met if the $a-b$ of background matrix has a slip-rate-dependent behavior, being less VW (Kaproth and Marone, 2013; Shibazaki and Iio, 2003) or VS (Fukuda et al., 2013; Sawai et al., 2017) with increasing loading rate. Therefore,

both SSEs and regular earthquakes can coexist on such a frictionally heterogeneous fault, and the distinctive factor of the long-term creeping and locked macrostructures is the spatial density of VW asperities and frictional properties of the creeping barrier (Corbi et al., 2017; Dublanchet et al., 2013; Nakata et al., 2011; Noda and Lapusta, 2013; Yabe and Ide, 2017) (Fig. 6).

In such a frictionally heterogeneous structure, an increase in shear stress caused by the SSEs is accommodated by the isolated failure of small to moderate-size asperities on the adjacent locked segment (Lay et al., 1982) (Fig. 6B). The efficient interaction between these small or moderate earthquakes, on the other hand, may generate enough stress perturbation through a domino effect and might occasionally lead to rupture of bigger asperities (Konca et al., 2008; Lay et al., 1982). The rupture on large asperities, in turn, could further grow laterally and break through nearby stressed asperities to form the source of the major earthquakes, such as the 2011 events (Corbi et al., 2017; Dublanchet et al., 2013) (Fig. 6B). However, the seismic asperities and barriers might not be permanent features, but instead, their size and space might vary within the megathrust depending on the slip and stress history (Konca et al., 2008; Park and Mori, 2007). This might explain the lack of a significant increase in seismic activity during some of the SSEs.

5. Conclusion

Here we constrained the time evolution of creep during the interseismic period of 1996–2003 on the northeastern Japan subduction zone. To this end, we used the creep estimates obtained from CRE observations in addition to the on-shore GPS displacement, corrected for common-mode and seasonal error. The obtained long-term coupling map reveals two main creeping sections to the north and south of the NJSZ, at depths larger than ~30 km, while the rest of megathrust, including the rupture zone of 2011 M_w9.0 earthquake is highly coupled during the interseismic period. Focusing on the northern creeping segment, we show the creep rate is not steady and instead evolves as a series of episodic SSEs. Quantified using the time series of released seismic moment, earthquake count, and Gutenberg-Richter *b*-value, we show that SSEs in the northern creeping segment are often accompanied by an increase in the seismic activity in their neighboring locked segment. This observation has a profound impact on the estimated seismic hazard in the region because it suggests a new triggering mechanism might exist, which acts across the megathrust on a range that was not known before.

Declaration of competing interest

The authors declare that they have no known competing financial interests or personal relationships that could have appeared to influence the work reported in this paper.

Acknowledgements

The authors are grateful to Felipe Aron and other reviewers for their comments and suggestions, which helped to improve the manuscript. We also thank S. Ozawa for sharing the GPS data. The Japan Meteorological Agency (JMA) earthquake catalog used in this study is available at www.jma.go.jp, subject to the policies of the JMA; **Funding:** This study was funded by National Science Foundation grants EAR-1357079 and EAR-1735630, NASA Earth and Space Fellowship No. 80NSSC17K0371, and JSPS KAKENHI grant 16H06473 and 15K05260.

Appendix A. Supplementary material

Supplementary material related to this article can be found online at https://doi.org/10.1016/j.epsl.2020.116261.

References

Apel, E.V., Bürgmann, R., Steblov, G., Vasilenko, N., King, R., Prytkov, A., 2006. Independent active microplate tectonics of northeast Asia from GPS velocities and block modeling. Geophys. Res. Lett. 33 (11), L11303. https://doi.org/10.1029/2006gl026077.

Avouac, J.P., 2015. From geodetic imaging of seismic and aseismic Fault slip to dynamic modeling of the seismic cycle. In: Jeanloz, R., Freeman, K.H. (Eds.), Annual Review of Earth and Planetary Sciences, vol. 43, pp. 233–271.

Bebout, G.E., Barton, M.D., 2002. Tectonic and metasomatic mixing in a high-T, subduction-zone melange - insights into the geochemical evolution of the slab-mantle interface. Chem. Geol. 187 (1–2), 79–106. https://doi.org/10.1016/s0009-2541(02)00019-0.

Bürgmann, R., Uchida, N., Hu, Y., Matsuzawa, T., 2016. Tohoku rupture reloaded? Nat. Geosci. 9 (3), 183. https://doi.org/10.1038/ngeo2649.

Chen, T., Lapusta, N., 2009. Scaling of small repeating earthquakes explained by interaction of seismic and aseismic slip in a rate and state fault model. J. Geophys. Res., Solid Earth 114, B01311. https://doi.org/10.1029/2008JB005749.

Corbi, F., Funiciello, F., Brizzi, S., Lallemand, S., Rosenau, M., 2017. Control of asperities size and spacing on seismic behavior of subduction megathrusts. Geophys. Res. Lett. 44 (16), 8227–8235. https://doi.org/10.1002/2017GL074182.

Davis, J.L., Wernicke, B.P., Tamisiea, M.E., 2012. On seasonal signals in geodetic time series. J. Geophys. Res., Solid Earth 117 (B1). https://doi.org/10.1029/2011jb008690.

Dieterich, J.H., 1979. Modeling of rock friction: 1. Experimental results and constitutive equations. J. Geophys. Res., Solid Earth 84 (B5), 2161–2168. https://doi.org/10.1029/JB084iB05p02161.

Dublanchet, P., Bernard, P., Favreau, P., 2013. Interactions and triggering in a 3-D rate-and-state asperity model. J. Geophys. Res., Solid Earth 118 (5), 2225–2245. https://doi.org/10.1002/jgrb.50187.

Fagereng, A., 2011. Fractal vein distributions within a fault-fracture mesh in an exhumed accretionary melange, chrystalls beach complex, New Zealand. J. Struct. Geol. 33 (5), 918–927. https://doi.org/10.1016/j.jsg.2011.02.009.

Fagereng, A., Sibson, R.H., 2010. Melange rheology and seismic style. Geology 38 (8), 751–754. https://doi.org/10.1130/g30868.1.

Fukuda, J.i., Kato, A., Kato, N., Aoki, Y., 2013. Are the frictional properties of creeping faults persistent? Evidence from rapid afterslip following the 2011 Tohoku-oki earthquake. Geophys. Res. Lett. 40, 3613–3617. https://doi.org/10.1002/grl.50713.

Gao, X., Wang, K.L., 2014. Strength of stick-slip and creeping subduction megathrusts from heat flow observations. Science 345 (6200), 1038–1041. https://doi.org/10.1126/science.1255487.

Gutenberg, B., Richter, C.F., 1944. Frequency of earthquakes in California. Bull. Seismol. Soc. Am. 34 (4), 185–188.

Hammond, W.C., Blewitt, G., Kreemer, C., 2016. GPS imaging of vertical land motion in California and Nevada: implications for Sierra Nevada uplift. J. Geophys. Res., Solid Earth 121 (10), 7681–7703. https://doi.org/10.1002/2016jb013458.

Harris, R.A., Segall, P., 1987. Detection of a locked zone at depth on the Parkfield, California, segment of the San-Andreas fault. J. Geophys. Res., Solid Earth Planets 92 (B8), 7945–7962. https://doi.org/10.1029/Jb092ib08p07945.

Hashimoto, C., Noda, A., Sagiya, T., Matsu'ura, M., 2009. Interplate seismogenic zones along the Kuril–Japan trench inferred from GPS data inversion. Nat. Geosci. 2, 141. https://doi.org/10.1038/ngeo421. https://www.nature.com/articles/ngeo421#supplementary-information.

Hayes, G.P., Wald, D.J., Johnson, R.L., 2012. Slab1.0: a three-dimensional model of global subduction zone geometries. J. Geophys. Res., Solid Earth 117 (B1), B01302. https://doi.org/10.1029/2011JB008524.

Heki, K., 2004. Space geodetic observation of deep basal subduction erosion in northeastern Japan. Earth Planet. Sci. Lett. 219 (1–2), 13–20. https://doi.org/10.1016/s0012-821x(03)00693-9.

Heuret, A., Conrad, C.P., Funiciello, F., Lallemand, S., Sandri, L., 2012. Relation between subduction megathrust earthquakes, trench sediment thickness and upper plate strain. Geophys. Res. Lett. 39, L05304. https://doi.org/10.1029/2011gl050712.

Hirose, H., Asano, Y., Obara, K., Kimura, T., Matsuzawa, T., Tanaka, S., Maeda, T., 2010. Slow earthquakes linked along dip in the Nankai subduction zone. Science 330 (6010), 1502. https://doi.org/10.1126/science.1197102.

Igarashi, T., 2003. Repeating earthquakes and interplate aseismic slip in the northeastern Japan subduction zone. J. Geophys. Res. 108 (B5). https://doi.org/10.1029/2002jb001920.

Ito, Y., Hino, R., Kido, M., Fujimoto, H., Osada, Y., Inazu, D., et al., 2013. Episodic slow slip events in the Japan subduction zone before the 2011 Tohoku-Oki earthquake. Tectonophysics 600, 14–26. https://doi.org/10.1016/j.tecto.2012.08.022.

Kaneko, Y., Avouac, J.-P., Lapusta, N., 2010. Towards inferring earthquake patterns from geodetic observations of interseismic coupling. Nat. Geosci. 3 (5), 363–U324. https://doi.org/10.1038/ngeo843.

Kaproth, B.M., Marone, C., 2013. Slow earthquakes, preseismic velocity changes, and the origin of slow frictional stick-slip. Science 341 (6151), 1229–1232. https://doi.org/10.1126/science.1239577.

Kato, A., Obara, K., Igarashi, T., Tsuruoka, H., Nakagawa, S., Hirata, N., 2012. Propagation of slow slip leading up to the 2011 m-w 9.0 Tohoku-Oki earthquake. Science 335 (6069), 705–708. https://doi.org/10.1126/science.1215141.

Khoshmanesh, M., Shirzaei, M., 2018a. Episodic creep events on the San Andreas fault caused by pore pressure variations. Nat. Geosci. 11 (8), 610–614. https://doi.org/10.1038/s41561-018-0160-2.

Khoshmanesh, M., Shirzaei, M., 2018b. Multiscale dynamics of aseismic slip on central San Andreas fault. Geophys. Res. Lett. 45 (5), 2274–2282. https://doi.org/10.1002/2018GL077017.

Khoshmanesh, M., Shirzaei, M., Nadeau, R.M., 2015. Time-dependent model of aseismic slip on the central San Andreas Fault from InSAR time series and repeating earthquakes. J. Geophys. Res., Solid Earth 120 (9), 6658–6679. https://doi.org/10.1002/2015JB012039.

Konca, A.O., Avouac, J.P., Sladen, A., Meltzner, A.J., Sieh, K., Fang, P., et al., 2008. Partial rupture of a locked patch of the Sumatra megathrust during the 2007 earthquake sequence. Nature 456 (7222), 631–635. https://doi.org/10.1038/nature07572.

Lay, T., Kanamori, H., Ruff, L., 1982. The asperity model and the nature of large subduction zone earthquakes. Earthqu. Predict. Res. 1, 3–71.

Leeman, J.R., Saffer, D.M., Scuderi, M.M., Marone, C., 2016. Laboratory observations of slow earthquakes and the spectrum of tectonic fault slip modes. Nat. Commun. 7, 11104. https://doi.org/10.1038/ncomms11104.

Liu, Y., Rice, J.R., 2007. Spontaneous and triggered aseismic deformation transients in a subduction fault model. J. Geophys. Res. 112 (B9). https://doi.org/10.1029/2007jb004930.

Loveless, J.P., Meade, B.J., 2010. Geodetic imaging of plate motions, slip rates, and partitioning of deformation in Japan. J. Geophys. Res. 115 (B2). https://doi.org/10.1029/2008jb006248.

Mavrommatis, A.P., Segall, P., Johnson, K.M., 2014. A decadal-scale deformation transient prior to the 2011 M-w 9.0 Tohoku-oki earthquake. Geophys. Res. Lett. 41 (13), 4486–4494. https://doi.org/10.1002/2014gl060139.

Meade, B.J., 2007. Algorithms for the calculation of exact displacements, strains, and stresses for triangular dislocation elements in a uniform elastic half space. Comput. Geosci. 33 (8), 1064–1075. https://doi.org/10.1016/j.cageo.2006.12.003.

Meneghini, F., Di Toro, G., Rowe, C.D., Moore, J.C., Tsutsumi, A., Yamaguchi, A., 2010. Record of mega-earthquakes in subduction thrusts: the black fault rocks of Pasagshak point (Kodiak Island, Alaska). Geol. Soc. Am. Bull. 122 (7–8), 1280–1297. https://doi.org/10.1130/b30049.1.

Meng, L.S., Inbal, A., Ampuero, J.P., 2011. A window into the complexity of the dynamic rupture of the 2011 Mw 9 Tohoku-Oki earthquake. Geophys. Res. Lett. 38, L00g07. https://doi.org/10.1029/2011gl048118.

Miyazaki, S.i., Larson, K.M., 2008. Coseismic and early postseismic slip for the 2003 Tokachi-oki earthquake sequence inferred from GPS data. Geophys. Res. Lett. 35 (4). https://doi.org/10.1029/2007GL032309.

Nadeau, R., Antolik, M., Johnson, P.A., Foxall, W., McEvilly, T.V., 1994. Seismological studies at Parkfield 3. Microearthquake clusters in the study of fault-zone dynamics. Bull. Seismol. Soc. Am. 84 (2), 247–263.

Nadeau, R.M., Johnson, L.R., 1998. Seismological studies at Parkfield VI: moment release rates and estimates of source parameters for small repeating earthquakes. Bull. Seismol. Soc. Am. 88 (3), 790–814.

Nakata, R., Ando, R., Hori, T., Ide, S., 2011. Generation mechanism of slow earthquakes: numerical analysis based on a dynamic model with brittle-ductile mixed fault heterogeneity. J. Geophys. Res., Solid Earth 116, B08308. https://doi.org/10.1029/2010jb008188.

Noda, H., Lapusta, N., 2013. Stable creeping fault segments can become destructive as a result of dynamic weakening. Nature 493 (7433), 518–521. https://doi.org/10.1038/nature11703.

O'leary, D.P., 1990. Robust regression computation using iteratively reweighted least-squares. SIAM J. Matrix Anal. Appl. 11 (3), 466–480. https://doi.org/10.1137/0611032.

Obara, K., Kato, A., 2016. Connecting slow earthquakes to huge earthquakes. Science 353 (6296), 253. https://doi.org/10.1126/science.aaf1512.

Ozawa, S., Nishimura, T., Munekane, H., Suito, H., Kobayashi, T., Tobita, M., Imakiire, T., 2012. Preceding, coseismic, and postseismic slips of the 2011 Tohoku earthquake, Japan. J. Geophys. Res., Solid Earth 117 (B7), B07404. https://doi.org/10.1029/2011jb009120.

Park, S.-C., Mori, J., 2007. Are asperity patterns persistent? Implication from large earthquakes in Papua New Guinea. J. Geophys. Res., Solid Earth 112 (B3). https://doi.org/10.1029/2006jb004481.

Perfettini, H., Ampuero, J.P., 2008. Dynamics of a velocity strengthening fault region: implications for slow earthquakes and postseismic slip. J. Geophys. Res., Solid Earth 113 (B9), B09411. https://doi.org/10.1029/2007jb005398.

Ruina, A., 1983. Slip instability and state variable friction laws. J. Geophys. Res., Solid Earth 88 (B12), 10359–10370. https://doi.org/10.1029/JB088iB12p10359.

Sagiya, T., 2004. Interplate coupling in the Kanto district, central Japan, and the Boso Peninsula silent earthquake in May 1996. Pure Appl. Geophys. 161 (11–12), 2327–2342. https://doi.org/10.1007/s0024-004-2566-6.

Sagiya, T., Miyazaki, S., Tada, T., 2000. Continuous GPS array and present-day crustal deformation of Japan. Pure Appl. Geophys. 157 (11/12), 2303–2322.

Savage, J.C., 1983. A dislocation model of strain accumulation and release at a subduction zone. J. Geophys. Res., Solid Earth 88, 4984–4996.

Sawai, M., Niemeijer, A.R., Hirose, T., Spiers, C.J., 2017. Frictional properties of JFAST core samples and implications for slow earthquakes at the Tohoku subduction zone. Geophys. Res. Lett. 44 (17), 8822–8831. https://doi.org/10.1002/2017gl073460.

Scholz, C.H., 1998. Earthquakes and friction laws. Nature 391, 37–42. https://doi.org/10.1038/34097.

Schorlemmer, D., Wiemer, S., Wyss, M., 2005. Variations in earthquake-size distribution across different stress regimes. Nature 437 (7058), 539–542. https://doi.org/10.1038/nature04094.

Schurr, B., Asch, G., Hainzl, S., Bedford, J., Hoechner, A., Palo, M., et al., 2014. Gradual unlocking of plate boundary controlled initiation of the 2014 Iquique earthquake. Nature 512 (7514), 299–302. https://doi.org/10.1038/nature13681.

Shakibay Senobari, N., Funning, G.J., 2019. Widespread fault creep in the northern San Francisco bay area revealed by multistation cluster detection of repeating earthquakes. Geophys. Res. Lett. 46 (12), 6425–6434. https://doi.org/10.1029/2019gl082766.

Shibazaki, B., Iio, Y., 2003. On the physical mechanism of silent slip events along the deeper part of the seismogenic zone. Geophys. Res. Lett. 30 (9). https://doi.org/10.1029/2003GL017047. 42-41 to 42-44.

Shibazaki, B., Matsuzawa, T., Tsutsumi, A., Ujiie, K., Hasegawa, A., Ito, Y., 2011. 3D modeling of the cycle of a great Tohoku-oki earthquake, considering frictional behavior at low to high slip velocities. Geophys. Res. Lett. 38 (21), L21305. https://doi.org/10.1029/2011gl049308.

Shirzaei, M., Bürgmann, R., 2013. Time-dependent model of creep on Hayward fault inferred from joint inversion of 18 years InSAR time series and surface creep data. J. Geophys. Res., Solid Earth 118, 1733–1746. https://doi.org/10.1002/jgrb.50149.

Shirzaei, M., Burgmann, R., Uchida, N., Hu, Y., Pollitz, F., Matsuzawa, T., 2014. Seismic versus aseismic slip: probing mechanical properties of the northeast Japan subduction zone. Earth Planet. Sci. Lett. 406, 7–13. https://doi.org/10.1016/j.epsl.2014.08.035.

Simons, M., Minson, S.E., Sladen, A., Ortega, F., Jiang, J., Owen, S.E., et al., 2011. The 2011 magnitude 9.0 Tohoku-Oki earthquake: mosaicking the megathrust from seconds to centuries. Science 332 (6036), 1421–1425. https://doi.org/10.1126/science.1206731.

Socquet, A., Valdes, J.P., Jara, J., Cotton, F., Walpersdorf, A., Cotte, N., et al., 2017. An 8 month slow slip event triggers progressive nucleation of the 2014 Chile megathrust. Geophys. Res. Lett. 44 (9), 4046–4053. https://doi.org/10.1002/2017gl073023.

Suwa, Y., Miura, S., Hasegawa, A., Sato, T., Tachibana, K., 2006. Interplate coupling beneath NE Japan inferred from three-dimensional displacement field. J. Geophys. Res., Solid Earth 111 (B4). https://doi.org/10.1029/2004jb003203.

Tanioka, Y., Ruff, L., Satake, K., 1997. What controls the lateral variation of large earthquake occurrence along the Japan Trench? Isl. Arc 6 (3), 261–266. https://doi.org/10.1111/j.1440-1738.1997.tb00176.x.

Tormann, T., Wiemer, S., Metzger, S., Michael, A., Hardebeck, J.L., 2013. Size distribution of Parkfield's microearthquakes reflects changes in surface creep rate. Geophys. J. Int. 193 (3), 1474–1478. https://doi.org/10.1093/gji/ggt093.

Uchida, N., Bürgmann, R., 2019. Repeating earthquakes. Annu. Rev. Earth Planet. Sci. 47 (1), 305–332. https://doi.org/10.1146/annurev-earth-053018-060119.

Uchida, N., Iinuma, T., Nadeau, R.M., Burgmann, R., Hino, R., 2016. Periodic slow slip triggers megathrust zone earthquakes in northeastern Japan. Science 351 (6272), 488–492. https://doi.org/10.1126/science.aad3108.

Uchida, N., Matsuzawa, T., 2013. Pre- and postseismic slow slip surrounding the 2011 Tohoku-oki earthquake rupture. Earth Planet. Sci. Lett. 374, 81–91. https://doi.org/10.1016/j.epsl.2013.05.021.

Wdowinski, S., Bock, Y., Zhang, J., Fang, P., Genrich, J., 1997. Southern California permanent GPS geodetic array: spatial filtering of daily positions for estimating coseismic and postseismic displacements induced by the 1992 Landers earthquake. J. Geophys. Res., Solid Earth 102 (B8), 18057–18070. https://doi.org/10.1029/97jb01378.

Yabe, S., Ide, S., 2017. Slip-behavior transitions of a heterogeneous linear fault. J. Geophys. Res., Solid Earth 122 (1), 387–410. https://doi.org/10.1002/2016jb013132.

Yamanaka, Y., Kikuchi, M., 2004. Asperity map along the subduction zone in northeastern Japan inferred from regional seismic data. J. Geophys. Res., Solid Earth 109 (B7), B07307. https://doi.org/10.1029/2003jb002683.

Yokota, Y., Koketsu, K., 2015. A very long-term transient event preceding the 2011 Tohoku earthquake. Nat. Commun. 6 (1), 5934. https://doi.org/10.1038/ncomms6934.